Swiss J Geosci (2015) 108:253–271
DOI 10.1007/s00015-015-0191-2

Burial history and thermal maturity of Mesozoic rocks of the Dolomites, Northern Italy

Arne Grobe[1] · Ralf Littke[1] · Victoria Sachse[1] · Detlev Leythaeuser[1]

Received: 6 August 2014 / Accepted: 8 May 2015 / Published online: 3 June 2015

Abstract Thermal maturity analyses provide a valid basis to reconstruct the burial and temperature history of sedimentary rocks. In combination with computer based modeling it is possible to quantify former overburden and erosional thickness. This study was carried out to analyze thermal maturity and elaborate the burial history of Permo-Mesozoic sediments of the Western Dolomites, Northern Italy. Based on their location in the non-metamorphosed Southern Alps of the Alpine realm, the Dolomites are well suited to study thermal maturation in a complex orogenic setting. Determination of maturity was carried out by vitrinite reflectance and solid bitumen reflectance measurements on a large number of samples as well as by Rock–Eval pyrolysis. Vitrinite reflectance commonly ranges between 0.5 % VR_r for Triassic and 0.76 % VR_r for Permian sediments allowing an analysis of the lateral and vertical maturation patterns. Several 1D basin models were developed and calibrated by maturity measurements. Results show that deepest burial probably occurred at the end of Cretaceous times, followed by erosion of about 1800 ± 200 m. The estimated heat flows were moderate with 75 mW/m^2 for Jurassic rifting, 46 mW/m^2 for times of deepest burial and 41 mW/m^2 for present day.

Keywords Alpine sedimentary units · Heat flow · Basin modeling · Erosion · Vitrinite reflectance · Solid bitumen reflectance

Editorial handling: E. Gnos.

✉ Arne Grobe
arne.grobe@emr.rwth-aachen.de

[1] Institute of Geology and Geochemistry of Petroleum and Coal, RWTH Aachen University, Lochnerstrasse 4-20, 52056 Aachen, Germany

1 Introduction

In sedimentary basin research, knowledge of the burial history is the key to reconstruct basin evolution.

With modern numerical modeling techniques it is possible to simulate and quantify the burial history of sedimentary basins (e.g. Bruns et al. 2013). As a prerequisite for numerical simulation, a good understanding of the geology, including lithology, thickness and stratigraphy is needed. Moreover, data representing the thermal history of the basin is required to calibrate and verify the simulated burial trends. Dispersed organic matter in sedimentary basins reacts strongly and irreversibly to temperature increase (Bostick and Foster 1975; Scheidt and Littke 1989). Thus, it is well suited for petrological and geochemical analyses revealing parameters that represent the maximum temperatures reached upon deep burial. A common parameter to analyze thermal maturity is the reflectance of dispersed organic matter, such as vitrinite or solid bitumen particles (e.g. Nöth et al. 2001; Schoenherr et al. 2007; Littke et al. 2012).

Within the Alps the Dolomites are characterized by a geological situation which favors this type of analysis of thermal and burial history. Deposits of various stratigraphic formations are still present in their original lateral continuity and intense folding, nappe thrusting and metamorphism, widespread in most alpine regions, did not occur in the area of the Dolomites (Doglioni 1987; Bosellini et al. 2003). This geological situation is clearly present in the western Dolomites, the study area of this work.

In the western Dolomites a Mesozoic sedimentary succession is underlain by thick layers of sedimentary rocks and volcanics of Permian age. This volcanic sheet prevented a stronger deformation of the area. The overlying Mesozoic column is represented by 2500 to 3000 m of

sedimentary rocks, mainly carbonates with interlayered shales (Bosellini 1998; Brandner et al. 2011).

In areas affected by uplift events during geological history the eroded thicknesses can be reconstructed on the basis of burial history modeling. For some alpine areas such uplift and erosional histories have been studied by analysis of apatite fission tracks (Central Alps: Bernet et al. 2001; Appenines: Dunkl et al. 2001; Venetian foreland: Zattin et al. 1990) or other maturity parameters, e.g. in Austria (e.g. Sachsenhofer 1992; Rantitsch et al. 2005), Switzerland (e.g. Suchy et al. 1997; Mählmann and Giger 2012) and Slovenia (Rainer et al. 2009). In the Dolomites only a few studies, partly published in German, focused on reconstruction of thermal maturity (Emmerich et al. 2005, 2008; Tscherny 2006; Tscherny et al. 2011; Blendinger et al. 2013). Tscherny et al. (2011) performed numerical modeling for the area east of the city of Corvara (Fig. 1) and estimated eroded thicknesses in the order of 1700–2400 m.

The objective of the present study is a reconstruction of the burial and uplift history of Mesozoic sediments and the evaluation of the eroded thicknesses of the Cretaceous layers for the northwestern Dolomites and a comparison with results from previous studies on other parts of the Dolomites. Three representative sections were chosen to evaluate the burial history by application of the PetroMod 1D software package (Schlumberger; Version 2012). Thermal maturity was analyzed by vitrinite and solid bitumen reflectance measurements to determine maximum burial depth. These data are essential for calibration of the modelled burial history. Additionally, elemental analysis and Rock–Eval pyrolysis were carried out in order to obtain information on petroleum generation and depositional conditions. This data set was interpreted in the context of previous studies on the evolution of the western Dolomites.

2 Geological setting and stratigraphy

The regional stratigraphy of the study area in the Dolomites (Fig. 1) comprises Permian to Cretaceous, but mainly Triassic rock units, underlain by a deformed Paleozoic basement metamorphosed during the Variscan Orogeny (Fig. 2, Bosellini et al. 2003). Initial rifting in the Early Permian produced thick volcanic layers (*Athesian Volcanic Group* or *Bozen Porphyry Plateau*) (Marocchi et al. 2008).

The sedimentary succession of the study area started in the Permian with the *Val Gardena Sandstone* (*Grödner*

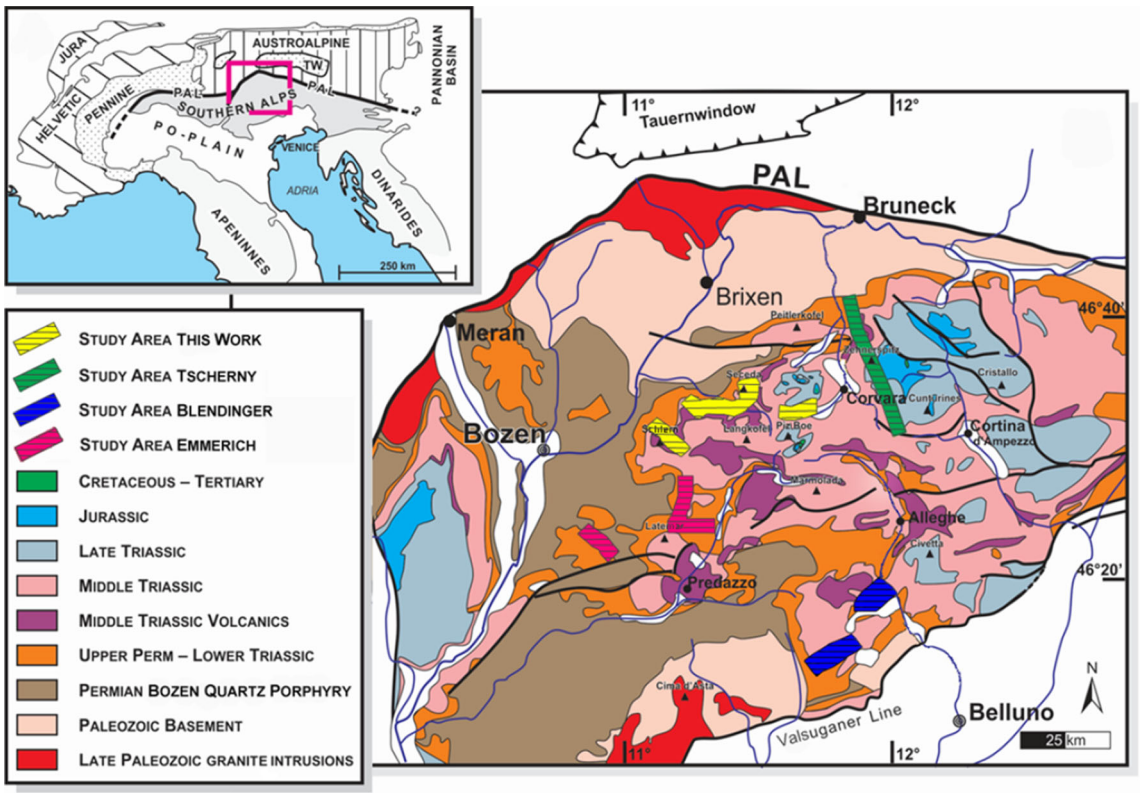

Fig. 1 Geological map of the Dolomites. The Dolomites are bordered by the Periadriatic Lineament (*PAL*) in the north and the Suganer Line in the south. *Highlighted* are the study areas of this and former vitrinite reflectance studies [Map after Brandner (1980) and Bigi et al. (1990), modified according to Tscherny (2006)]

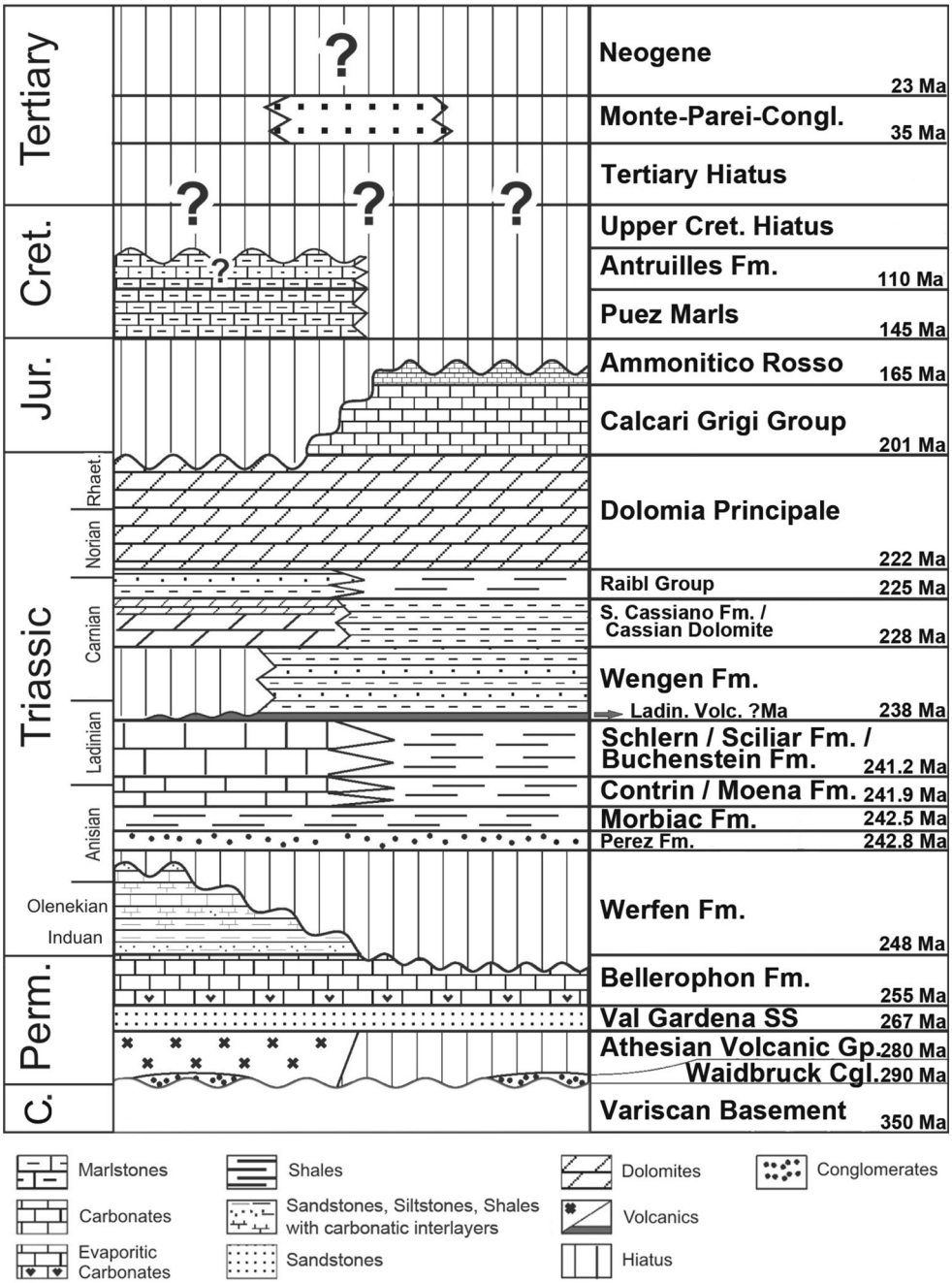

Fig. 2 Simplified stratigraphy of the Dolomites in the Val Gardena area. Listed ages and stratigraphies are used in the numerical model. Modified after Tscherny et al. (2011). Compiled from Bosellini (1998), Keim et al. (2001) and Bosellini et al. (2003). Ages from Mundil et al. (2010) and Ogg et al. (2014)

Sandstein), representing red beds of a semi-arid paleo setting, covered by shallow marine evaporites and carbonates (*Bellerophon Formation*) (Massari and Neri 1997; Bosellini et al. 2003) towards the end of the Permian. They are unconformably covered by shallow-water carbonates and interbedded terrigenous deposits of the Lower Triassic *Werfen Formation*. After uplift and local deposition of terrestrial clastic sediments (*Perez Fm.*, locally used unit, as Voltago Conglomerate and Richthofen Conglomerate are not clearly distinguishable in the study area) renewed transgression in the western part resulted in lagoonal deposits comprised of terrigenous siliciclastics and carbonates of the *Morbiac Fm.* Then first carbonate platforms developed in shallow marine areas (*Contrin Fm.*).

During the Late Anisian a fast subsidence pulse was associated with platform drowning and contemporaneous quick upward aggradation (Stefani et al. 2010). Thereby, huge carbonate platforms (*Sciliar/Schlern Fm.*) were produced, with deep basin sediments deposited in between (*Buchenstein Fm.*). Platform examples are the Marmolata and Catenaccio (Rosengarten) complexes.

During the tectono-magmatic event of Ladinian age, some platforms were penetrated by dykes and large volcanic collapses occurred (Bosellini et al. 2003). Volcanic, erosional debris with interlayered, calcareous detritus was subsequently deposited in the basin facies (*Wengen Fm.,* Fig. 2) (Keim 2008). The San Cassiano Formation (Keim 2008) represents a continuous sedimentation of calcareous basin fill lacking any volcanic detritus. As basinal platform the *Cassian Dolomite* developed on top of it, overlain by shallow marine to continental depostits of the *Raibl Group* (Stefani et al. 2010).

Subsequently, a massive carbonate platform (*Dolomia Principale*) developed due to slow but continuous subsidence (Hardie and Goldhammer 1986; Blendinger 2004; Emmerich et al. 2005).

Towards the end of the Norian (Late Triassic), the dry, arid climate changed to wet climate (Bosellini 1998; Berra et al. 2010). A slow plateau subsidence, resulted in the change from the deposition of the shallow marine Calcari Grigi deposition to deeper-water sedimentation of slumps and redeposited pelagic sediments of the Ammonitico Rosso (Bertotti et al. 1993; Masetti et al. 2012). The present day thicknesses of the Calcari Grigi and the Ammonitico Rosso are varying in the study area: East of the *Val Badia* Triassic deposits are followed without any hiatus by Jurassic sediments. However, the Jurassic is completely missing or preserved only as very thin and partly eroded layer on the western site of the valley. In the latter area the Cretaceous *Puez-Marls* follow unconformably above the Triassic *Dolomia Principale* (Tscherny 2006).

With the opening of the Ligurian-Piedmontese ocean in the Middle to Upper Jurassic a new system of rifting evolved (Bertotti et al. 1993) and the area of the Eastern Dolomites became a passive continental margin (Carminati et al. 2010). Nevertheless, the area was affected by ongoing subsidence during the Upper Jurassic and Cretaceous (Winterer and Bosellini 1981). At the end of the Jurassic the depositional system changed to a more pelagic-clastic one with calcarenites and mud turbidites (Carminati et al. 2010).

The stratigraphy of the Cretaceous is complex, but almost all the Cretaceous is documented at different places of the Dolomites. In the summit region of the Gardenaccia, only the lower Cretaceous is preserved (Maiolica and Puez Marls) above very thin Jurassic units (Stock 1994). However, in the Sella group Cretaceous sediments follow conformably above the Ammonitico Rosso or above an erosional surface within the Dolomia Principale. In the northern Dolomites, in the Fanes-Sennes area, the Upper Cretaceous units are very well known and the succession spans from Maiolica (Tithonian to Barremian) to Scaglia Rossa (Antruilles Fm, Turonian–Maastrichtian).

In the Val Gardena area the only Cretaceous sediments preserved are the above mentioned of the Puez-Marls (Bosellini 1998; Lukeneder and Aspmair 2006; Lukeneder 2010). All other Cretaceous sediments were eroded during the Late Cretaceous and/or Tertiary (Fig. 2) due to the uplift of the Alps (Doglioni 1984, 1992; Carminati and Doglioni 2012). Apart from the Mont-Parei-Conglomerate, Tertiary deposits are not preserved in the study area and the Quaternary is represented only by thin sediment fillings of Alpine valleys.

3 Samples and methods

Sample coverage of maturity measurements by selected previous publications (Tscherny 2006; Emmerich et al. 2008; Blendinger et al. 2013) is shown in Fig. 1. In combination with the previously assembled data set, an improved database was achieved as a solid basis for numerical basin modeling.

Based on fieldwork and literature information, the following stratigraphic layers were identified as potentially vitrinite-bearing: *Val Gardena Fm., Wengen Fm., Heiligkreuz Fm., Moena Fm.* (Bosellini 1998; Tscherny 2006), *Buchenstein Fm., Morbiac Fm*. and the *Upper Bellerophon Fm.* (Bosellini et al. 2003). Among those, the two first listed formations were classified as "good" and the remaining ones as "medium"-quality using the quality criteria of vitrinite reflectance measurements (Tscherny 2006). He classified samples as "good-quality" provided they allowed the identification of more than 30 vitrinite particles for reflectance measurements, whereas samples with fewer vitrinite particles were termed "medium-quality". In each of these formations the interlayered, laminated and marly layers are best suited. Locations close to intrusions and volcanic dykes were avoided in order to exclude local thermal overprinting of organic matter maturity.

These considerations led to the selection of two areas for fieldwork and sampling. The first area is the Gardena Valley (ital. *Val Gardena*.) between St. Ullrich (*Ortisei/Urtijei*) and Wolkenstein (*Selva Gardena*), approximately 25 km northeast of the city of Bozen. The second area of interest is the *Frötschbach* area, approximately 3 km southeast of the village of Seis (see "Appendix Table 4" for sample coordinates).

In the Gardena Valley, 43 samples were collected from three sections. In all of them the stratigraphic units from *Bellerophon* to *Buchenstein* are cropping out. Mainly the *Buchenstein Formation,* and the *Bulla Member* of the *Upper Bellerophon Fm*. were sampled.

Apart from these three sections the following additional Buchenstein Fm. samples were collected: four from the

Seceda, one from the *Würzjoch* and 12 from the eastern continuation of the *Gardena Valley*, north of the city of *Colfosco.*

In the *Frötschbach* area two sections were sampled; one in the valley of the *Frommerbach,* where the complete stratigraphic sequence from the *Perez Fm.* to the *Wengen Fm.* is cropping out. Another section was sampled on the slopes of the *Frötschbach* valley itself.

A total number of 153 samples was collected from outcrop sections, whereby fresh and visibly unweathered material was chosen. For characterization of elemental composition 37 dark-colored samples were selected for analysis of total organic and inorganic carbon (TOC, TIC). From this group 23 were also analyzed for total sulfur content (TS). For elemental analyses, 100 mg of each pulverized sample was combusted using a liquiTOC II analyzer to determine the total organic and inorganic carbon content. The instrument is using a temperature ramp method, which enables a direct determination of TOC and TIC without prior acidification of the samples (heating in two steps: 300 °C/min to 550 °C and held for 600 s, than raised to 1000 °C and held for 400 s). Under constant oxygen supply the organic carbon (first step) and the inorganic, carbonate carbon (second step) will generate CO_2, which is analyzed by a non-dispersed infrared detector (NDIR: detection limit 10 ppm, rel. TOC error 0.6 %, TIC error 1.7 %).

Based on this data $CaCO_3$ and $CaMg(CO_3)_2$ contents are calculated for all samples as follows:

$$CaCO_3 = TIC \cdot 8.333$$

$$CaMg(CO_3)_2 = TIC \cdot 7.667$$

Sulfur (total sulfur, TS) was measured on a LECO S200. After covering 100 mg of sample with Fluorhib and Fe-cuttings, it is combusted under constant oxygen supply in a high frequency induction furnace at 1000 °C. During this procedure sulfur is oxidized to SO_2. The generated gases are flashed by the carrier gas oxygen through a water trap to remove water vapor and then to a SO_2-specific infrared cell to measure the total sulfur content (detection limit 20 ppm, relative error <5 %).

Thermal maturity was characterized by vitrinite and solid bitumen reflectance measurements. Samples selected on the basis of their color and TOC content were prepared for organic petrological analysis. Samples cut perpendicular to bedding were impregnated with a mixture of epoxy-resin (Scandiplex A) and a hardener (Scandiplex B). During the exothermal hardening maximum temperatures did not exceed 36 °C. Each block was polished on one side with successively finer abrasives (320, 400, 600 mm; see Littke et al. 2012; Sachse et al. 2012 for more details).

Reflectance measurements were performed on an incident light microscope Zeiss Axioplan with an oil immersion lens of 50-times magnification under monochromatic light with a wavelength of 546 nm. Oil with known refractive index was used to avoid undesired diffusion reflectance (Taylor et al. 1998). The microscope was calibrated with an yttrium–aluminum–garnet-standard (YAG) with a constant reflectance of 0.889 %; this standard can be used up to values of 1.3 % VR_r. According to Senftle et al. (1993) measurement of at least 30 vitrinite particles should be made to obtain a representative mean value. Due to a lack of vitrinites, this number was not reached for some of the samples.

Vitrinite reflectance data can be used to characterize a broad range of maturities, from early diagenesis (~0.2 % VR) up to low grades of metamorphism (~>4.0 % VR) in order to determine maximum burial depth (Sweeney and Burnham 1990; Barker and Pawlewicz 1994). As a first estimation, maximum temperatures of burial heating were calculated based on the following formula by Barker and Pawlewicz (1994):

$$T_{peak} = \frac{\ln(VR_r) + 1.68}{0.0124}$$

In many cases two maxima of vitrinite reflectance values are observed. In such cases, the lower reflectance values normally represent the autochthonous vitrinites since the higher maximum usually represents resedimented, allochthonous particles (Taylor et al. 1998). Solid bitumen reflectance (BR_r) can be measured if vitrinites are not observed, e.g. in pre-Devonian rock or rocks containing little terrestrial material. Measured values reflect thermal maturity and can be converted into vitrinite reflectance by the formula of Schoenherr et al. (2007):

$$VR_r\,(\%) = \frac{(BR_r + 0.2443)}{1.0495}$$

To obtain VR_r vs. depth trends from field data without expensive drilling campaigns pseudowells were created according to the method of Nöth et al. (2001). Therefore, sediments of different formations were sampled at the surface and measured for VR_r and BR_r. Results were extrapolated into a VR_r vs. pseudo-depth profile perpendicular to bedding.

Based on their TOC values 9 samples were selected for Rock–Eval analysis to characterize the quality of organic matter. 100 mg of each pulverized sample was treated according to Espitalié et al. (1985).

The temperature of the generated maximum S2 yield (T_{max}) was used as another maturity parameter. According to Hunt (1995) "the hydrogen index (S2 normalized to TOC) could be roughly correlated with the atomic H/C ratio and the oxygen index with the atomic O/C ratio of the

van Krevelen diagram". Thus, in a Hydrogen Index (HI) versus Oxygen Index (OI) diagram kerogen quality can be interpreted in a similar way as in the well-known van Krevelen plot. Due to problems with a strong mineral-matrix-effect in the case of low TOC values, only samples with TOC contents in excess of 0.5 wt% were selected for analyses (Saeed and Peters 1994).

To quantify maximum burial temperature and depth integrated basin modeling was performed for the two study areas with the PetroMod1D 2012.1 software package, developed by the Schlumberger Technology Center Aachen, Germany. The software uses a forward modeling, event-stepping approach. In this way, the simulation starts with the deposition of the oldest sediment layer and continues with decreasing geological age of the strata, event by event, until the present-day geometry of the sediment-fill is reached.

As a first step, a generalized present-day stratigraphic column of the studied sections needs to be defined, including lithologies, petrophysical data, depositional ages and thicknesses of all units. This so called conceptional model is based on a chronology of events, i.e. sedimentation, erosion, hiatus (non-deposition) and tectonic events (e.g., salt movement/doming, volcanism, thrusting).

Thermal boundary conditions are needed to define the overall thermal regime of the sedimentary basin over time. The two main input parameters are the basal heat flow [HF (mW/m^2), lower thermal boundary] and the paleo water depth [PWD (m), upper boundary]. The PWD is used to calculate the sediment water interface temperature [SWIT (°C)] (Hantschel and Kauerauf 2009). Furthermore, internal radiogenic heat production is calculated based on sedimentary lithologies depending on their average abundance of uranium, thorium and potassium.

For each buried layer the software calculates vitrinite reflectance according to the EASY $\%R_0$ method of Sweeney and Burnham (1990). This calculated VR value is compared with the measured VR value and the model is adjusted until a best fit of the VR vs. depth trend is achieved.

4 Results and discussion

4.1 Elemental analysis

Results of the elemental analyses are listed in Table 1 and plotted in Fig. 3. The samples show a wide range of TOC, even within a single formation (Fig. 3a). TOC values range from a shaly limestone with 2.3 % (13/696) to a red shale with 0.01 % (13/639). Most samples vary between 0.3 and 1.8 % TOC and a weak correlation of TOC and lithology is observed. Limestones with interbedded shales (shaly limestone) range between 1.1 (13/653) and 2.3 % TOC (13/696), whereas purer limestones are characterized by lower TOC values between 0.3 (13/660) and 0.8 % (13/677).

Calculated carbonate contents vary between 6.3 (13/699) and 115.7 % (13/745, based on calculation of calcite content). Data exceeding 100 % are explained by a significant contribution of dolomite rather than calcite (Table 1).

Measurement of total sulfur content (TS) allows to characterize the depositional environment (Fig. 3b, Berner 1984; Lückge et al. 1999, 2002). Values for total sulfur contents vary between nearly 0 and 0.95 wt%.

Figure 3b shows that most samples plot below the normal marine trend (Berner 1984). Two samples (13/666, 13/684) show much higher TS/TOC ratios. This can be explained by the influence of oxygen-free bottom waters and/or the occurrence of late diagenetic pyrite (FeS_2). The occurrence of pyrite was documented for all samples by microscopic examination. Low sulfur contents, e.g. within the *Wengen* or *Perez Fm.*, may indicate the influence of weathering (Littke et al. 1991), which is not the case here, as the pyrite is fresh.

4.2 Organic petrology

Vitrinites are organic particles derived from woody tissues of higher land plants, mainly originating from lignin and cellulose of plant cell walls (Taylor et al. 1998). During burial and coalification chemical and physical changes take place, which are temperature dependent and irreversible. Especially, with increasing thermal maturation vitrinite becomes more aromatized (Schenk et al. 1990) and as a consequence its ability to reflect light increases. Therefore, vitrinite reflectance can be used to determine the thermal maturity of the organic matter in sedimentary rocks. In most cases vitrinite reflectance increases exponentially with a linear increase of temperature (amongst others: Ting 1973; Saxby et al. 1986). Due to the fact that coalification is irreversible, the maximum temperature a rock has experienced is archived in the reflectance of vitrinites in sedimentary rocks.

For 46 samples reflectance was measured: 42 of them contain vitrinites and four solid bitumen ("Appendix Table 4"). In four samples neither vitrinites nor solid bitumen has been detected (13/643, 13/688, 13/710 and 13/711). New obtained data (this study) were compared to literature data from other parts of the Dolomites (Buggisch 1978; Schulz and Fuchs 1991; Bielefeld 1998; Tscherny 2006; Emmerich et al. 2008; Blendinger et al. 2013). Thus, a total number of 75 samples with vitrinite reflectance values is available ("Appendix Table 4"). They range from immature (e.g. from 0.37 % VRr to 0.60 % VRr) to post-mature (up to 1.75 % VR_r, 13/681) stages (classification

Table 1 $CaCO_3$ and $CaMg(CO_3)_2$ calculated from TIC

Sample no.	Formation	TOC (wt%)	TIC (wt%)	$CaCO_3$ (%)	$CaMg(CO_3)_2$ (%)	TS (%)
13/666	Wengen	0.39	2.33	19.4	17.9	0.57
13/761	Wengen	1.21	1.43	11.9	11.0	–
13/762	Wengen	1.20	2.21	18.4	17.0	–
13/705	Buchenstein	0.19	6.70	55.8	51.4	0.13
13/699	Buchenstein	1.36	0.76	6.3	5.8	0.48
13/698	Buchenstein	1.74	1.40	11.7	10.7	0.85
13/696	Buchenstein	2.28	2.51	20.9	19.2	0.95
13/687	Buchenstein	0.18	2.77	23.1	21.2	0.04
13/680	Buchenstein	0.09	2.62	21.8	20.1	0.01
13/679	Buchenstein	0.30	2.49	20.7	19.1	0.03
13/678	Buchenstein	0.18	3.22	26.8	24.7	0.03
13/677	Buchenstein	0.75	5.35	44.6	41.0	0.05
13/664	Buchenstein	0.09	2.89	24.1	22.2	0.03
13/662	Buchenstein	0.12	6.15	51.2	47.1	0.03
13/660	Buchenstein	0.32	3.03	25.2	23.2	0.06
13/653	Buchenstein	1.12	3.23	26.9	24.8	0.03
13/651	Buchenstein	1.72	5.23	43.6	40.1	0.12
13/650	Buchenstein	0.15	11.42	95.2	87.6	0.01
13/751	Buchenstein	0.18	6.86	57.1	52.6	–
13/753	Buchenstein	0.10	8.76	73.0	67.2	–
13/754	Buchenstein	0.07	9.01	75.1	69.1	–
13/683	Contrin	0.09	13.55	112.9	103.9	<0.01
13/684	Morbiac	0.19	7.15	59.6	54.8	0.59
13/746	Morbiac	0.09	13.62	113.5	104.4	–
13/747	Morbiac	0.09	13.37	111.4	102.5	–
13/748	Morbiac	0.02	13.74	114.5	105.4	–
13/749	Morbiac	0.16	11.67	97.3	89.5	–
13/750	Morbiac	0.06	13.88	115.6	106.4	–
13/639	Perez	0.01	5.17	43.1	39.6	0.01
13/744	Bellerophon	0.86	13.51	112.6	103.6	–
13/745	Bellerophon	1.22	13.88	115.7	106.4	–
13/755	Bellerophon	0.03	13.01	108.4	99.8	–
13/756	Bellerophon	0.12	11.08	92.3	85.0	–
13/656	Bellerophon	1.74	5.91	49.2	45.3	0.1
13/655	Bellerophon	0.68	11.27	93.9	86.4	0.17
13/635	Bellerophon	1.40	10.37	86.4	79.5	0.08
13/634	Bellerophon	0.01	10.41	86.7	79.8	0.02

according to Peters et al. 2005). Most data represent samples from within the oil window, below or at peak oil generation (41 samples, 0.60–0.90 % VR_r). Only six samples are characterized as immature and 24 samples are interpreted as late mature (0.90–1.35 VR_r). The latter ones are interpreted as overprinted by Ladinian volcanic intrusions and are marked (^{v}) in the table of the Appendix. Also, samples are marked (^{std}) for which the variation of measured values, i.e. the standard deviation, is very high, resulting in less reliable information as compared to the remaining samples.

The whole area of the *Gardena Valley/Val Gardena* shows mature vitrinites (0.61–0.75 % VR_r) at all sampled locations with a more or less normally increasing depth trend (VR vs. depth trend established by a plot of measured VR versus the stratigraphic position of each sample). The study area around the *Frötsch- and Frommerbach* indicates the same trend with mature to late mature samples (0.50–0.92 % VR_r). Similar results are observed in the *Colfosco* area with mature to late mature range (0.73–0.96 % VR_r).

The VR data of the *Buchenstein Fm.* indicate slightly increasing values from east to west and also from north to south.

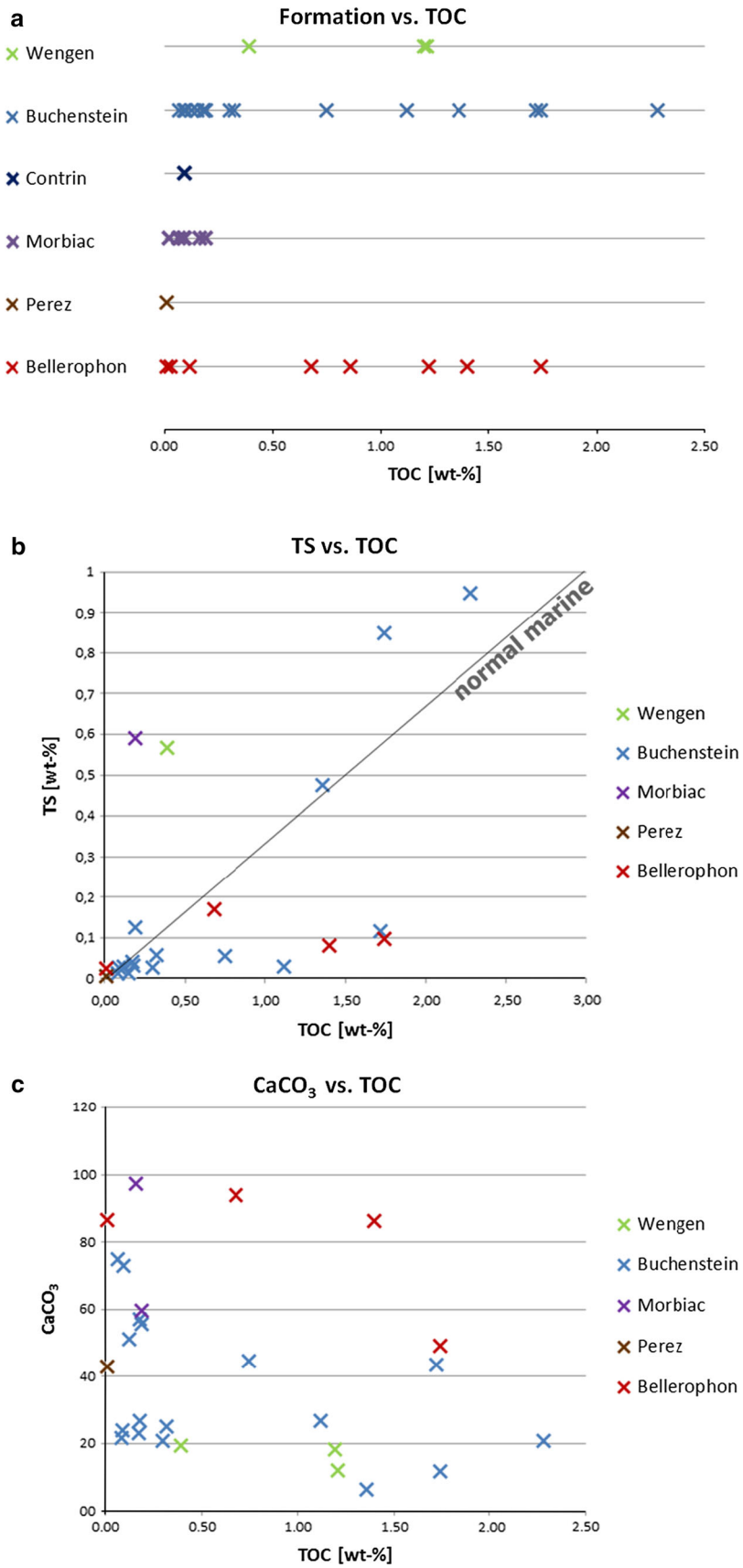

Fig. 3 Plots of analysis data: **a** TOC values of studied formations, **b** TS vs. TOC. *Black line* represents normal marine conditions (after Berner 1984), and **c** TOC vs. $CaCO_3$ contents

Table 2 Rock–Eval pyrolysis and TOC data

Sample no.	Formation	TOC (wt%)	S1 (mg/g rock)	S2 (mg/g rock)	S3 (mg/g rock)	T_{max} (°C)	HI (mg HC/gTOC)	OI (mg CO_2/gTOC)	PI (–)	Notes
13/635	Bellerophon	1.40	0.13	0.92	1.41	446	66	101	0.12	S2 peak wide
13/651	Buchenstein	1.72	0.52	5.25	0.73	442	305	43	0.09	
13/653	Buchenstein	1.12	0.23	1.23	0.97	442	110	87	0.16	
13/655	Bellerophon	0.68	0.27	0.77	0.89	451	114	131	0.26	
13/656	Bellerophon	1.74	0.15	1.07	2.18	451	62	126	0.12	S2 peak wide
13/677	Buchenstein	0.75	0.13	1.01	0.88	444	134	117	0.12	
13/696	Buchenstein	2.30	0.35	8.06	1.10	425	350	48	0.04	
13/698	Buchenstein	1.74	0.30	7.46	0.66	430	428	38	0.04	
13/699	Buchenstein	1.36	0.24	4.25	0.84	428	312	62	0.05	

4.3 Rock–Eval pyrolysis

Based on their TOC values, 9 samples were selected for Rock–Eval pyrolysis. Table 2 shows the results. According to Hunt (1995), "The most important factor controlling the generation of oil and gas is the hydrogen content of the organic matter (OM)". Here, Hydrogen Index values vary between 62 and 428 mg HC/g TOC. Oxygen Index values range between 38 and 131 mg CO_2/g TOC. To illustrate the results HI and OI are plotted in the pseudo-van Krevelen diagram in Fig. 4. Samples 13/651, 13/696, 13/698 and 13/699 of the *Buchenstein Fm.* can be characterized as containing Type II kerogen. Their low PI values indicate either that these source rocks have expelled petroleum, or alternatively, they may result from weathering (Littke et al. 1991). The high S2 peaks show that burial temperature never reached the peak oil generating stage (Rullkötter et al. 1988).

All other samples can be characterized as bearing Type III kerogen, indicating a terrigenous origin of the organic matter. It should be noted that due to the analyses of whole rock samples, instead of pure kerogen samples, the OI values might be overestimated and the HI underestimated (Peters 1986).

T_{max} values range from 425 to 451 °C and basically agree with maturity information based on vitrinite reflectance data. Nevertheless, minor discrepancies are observed, e.g. samples 13/696 and 13/699 show low T_{max} values, although vitrinite reflectance values are at 0.7 %.

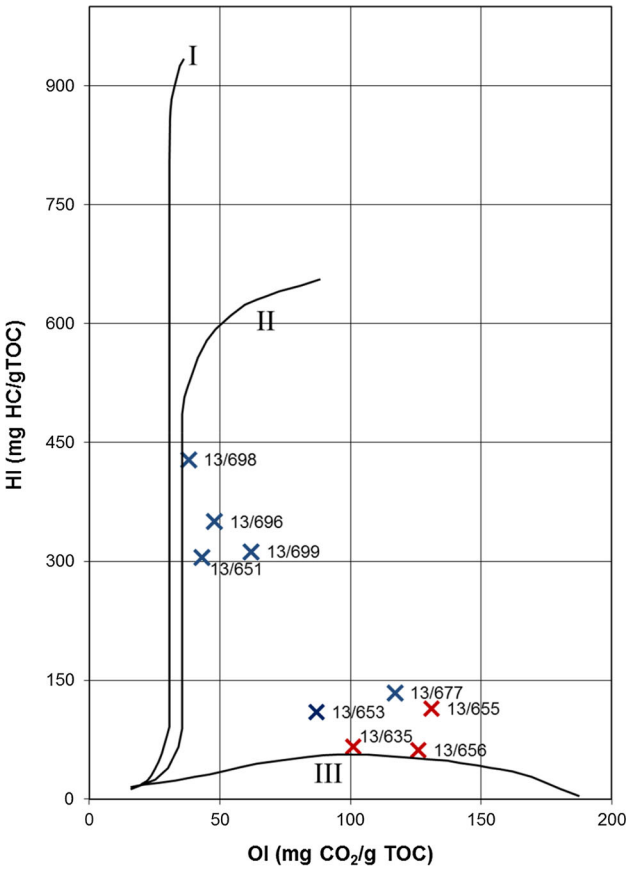

Fig. 4 HI vs. OI plot of the Rock–Eval VI data (Buchenstein Fm. *blue x*, Bellerophon *red x*). The *lines* represent medians of the kerogens types *I–III* and are based on Espitalié et al. (1985)

4.4 Thermal history modeling

The stratigraphy used as input for the simulation is shown in Table 3. It was compiled from Bosellini (1998), Bosellini et al. (2003) and Keim et al. (2001). The model includes 21 layers ranging in age from the Bozen Quartz Porphyry of the Athesian Volcanic Group to Quaternary sediments. Thicknesses were modified after Tscherny (2006) and the absolute ages are from Ogg et al. (2014) supplemented by data of Mundil et al. (1996, 2010). The relevant lithologies (Table 3) have been built with the PetroMod Lithology Editor and are based on field observations as well as descriptions of Bosellini (1998). For

Table 3 Stratigraphy used as fixed input for the simulation

Formation	Present thickness (m)	Eroded thickness (m)	Start of deposition (Ma)	End of deposition (Ma)	Start of erosion (Ma)	End of erosion (Ma)	Lithology
Quaternary	10		0.20	0.00			Marl + Shale + Silt + SS
Monte-Parei_Fm.	0	50	35.00	33.00	33.00	20.00	Sandstone + Conglomerate
Belluno-Flysch	0		65.00	49.00			Sandstone_silty
Cretaceous_Hiatus	0	?	120.00	65.00	43.00	40.20	Sandstone + Silt
Antruilles_Fm.	0	50	110.00	120.00	40.20	40.00	Sandstone (silty_organic)
Puez_Marls	0	150	145.00	110.00	40.00	39.00	Marl
Ammonitico_Rosso	0	20	165.00	155.00	155.00	154.00	Limestone_shaly
Calcari_Grigi_Group	0	500	201.00	165.00	154.00	151.00	Limestone_shaly
Dolomia_Principale	0	500	222.00	201.00	151.00	148.00	Dolomite (typical)
Raibler Group	0	50	225.00	222.00	148.00	147.50	Marl
S_Cassiano/Cassian Dolomite	0	300	228.00	225.00	142.00	145.00	Marl
Wengen_Fm._incl_volcanics	400		238.00	228.00			Sandstone_shaly
Buchenstein/Schlern/ Sciliar_Fm.	60		241.20	238.00			Limestone_shaly
Contrin/Moena_Fm.	140		241.90	241.20			Dolomite + SS + Silt
Morbiac_Fm.	20		242.50	241.90			Marl + Shale + Silt + SS
Perez_Fm.	30		242.80	242.50			Sandstone + Conglomerate
Werfen_Fm.	180	220	252.00	244.00	244.00	242.80	Marl + Shale + Silt + SS
Bellerophon_Fm.	200		255.00	252.00			Limestone + Evap + Gypsum + Shale
Val-Gardena-Sandstone_Fm.	200		267.00	255.00			Sandstone (silty_org)
Athesian Volcanic Group	1000		350.00	290.00			Rhyolite_(tuff_frag)

Additionally, the present day and the eroded thicknesses of each formation are listed, as well as deposition and erosion ages and lithologies. An estimation of the thickness of the Cretaceous erosion will be part of this work; hence, it is marked with a question mark (?)

periods of uplift fixed thickness values for eroded strata are used with the exception of the Cretaceous/Tertiary erosion. The thickness of sediments eroded during Cretaceous/Early Tertiary was derived from modeling results. Short-term erosion events occurred during the Early Triassic and the Miocene. It should be noted that the timing of erosion of Triassic to Cretaceous formations is largely unknown and arbitrary values are shown in Table 3. Our model reveals the total eroded thickness only as it is based on one single erosional event.

For the conceptional model six different phases were initially defined: (1) Sedimentation from 267 to 244 Ma (Val Gardena SS to Werfen Fm.), (2) erosion of parts of the Werfen Fm. 244–242.8 Ma, (3) sedimentation from 242.8 to 155 Ma (Perez Fm. to Rosso Ammonitico Fm.), (4) erosion from 155 to 145 Ma (S. Cassiano Fm. to Ammonitico Rosso. completely eroded), (5) sedimentation of Puez Marls, Antruilles Fm. and Upper Cretaceous (145–65 Ma), and (6) uplift, Alpine Orogenesis and erosion from 65 Ma until present with contemporaneous sedimentation of thin Cenozoic sediments in parts of the area.

With respect to the thermal evolution of the basin a general heat flow of 65 mW/m^2 was chosen as the base of the model, representing an average global heat flow value. Moreover, the following four thermal periods were defined (Fig. 5): (1) Rifting of the continental crust with Ladinian tectono-magmatic event in the early Middle Triassic (max heat flow: 65 mW/m^2), (2) opening of the Ligurian-Piemontese ocean and generation of oceanic crust in Middle and Upper Jurassic (max heat flow: 75 mW/m^2), (3) consolidation phase with crustal thickening starting in Upper Jurassic (cooling), (4) since Eocene, crustal thickening due to Meso- and Neoalpine orogenesis.

Based on this scenario the heat flow (HF) vs. time trend shown in Fig. 5 was generated. Fission track data interpretation of Tscherny (2006) was used to link time and temperature data (max. temperatures 100–110 °C in the Cretaceous, rapid cooling in the Eocene). Values for the period of Ladinian volcanism are relatively low since all samples were taken in areas without volcanic influence. The paleo water depth curve (PWD) shows an assumed fluvial to shallow marine evolution from the beginning of the Middle Triassic to the Cretaceous. Sediment water interface temperature was influenced by palaeolatitude as well as water depth during deposition. Deeper water with cooler temperatures characterizes sedimentation of the Buchenstein and Wengen Formation. The minimum temperature in the Middle Triassic is due to the rapid drowning of the carbonate platforms from tropical surface temperatures to cold deep sea water (Bosellini et al. 2003). The thermal evolution of the basin fill is strongly controlled by rock properties such as thermal conductivity, heat capacity and radiogenic heat production. VR depth trends for all 1D-pseudowells were generated to study temperature history. Since the simulations of all pseudo-wells show similar trends, only the *Gardena Valley* model is described and discussed here in detail. Results of the sensitivity analyses

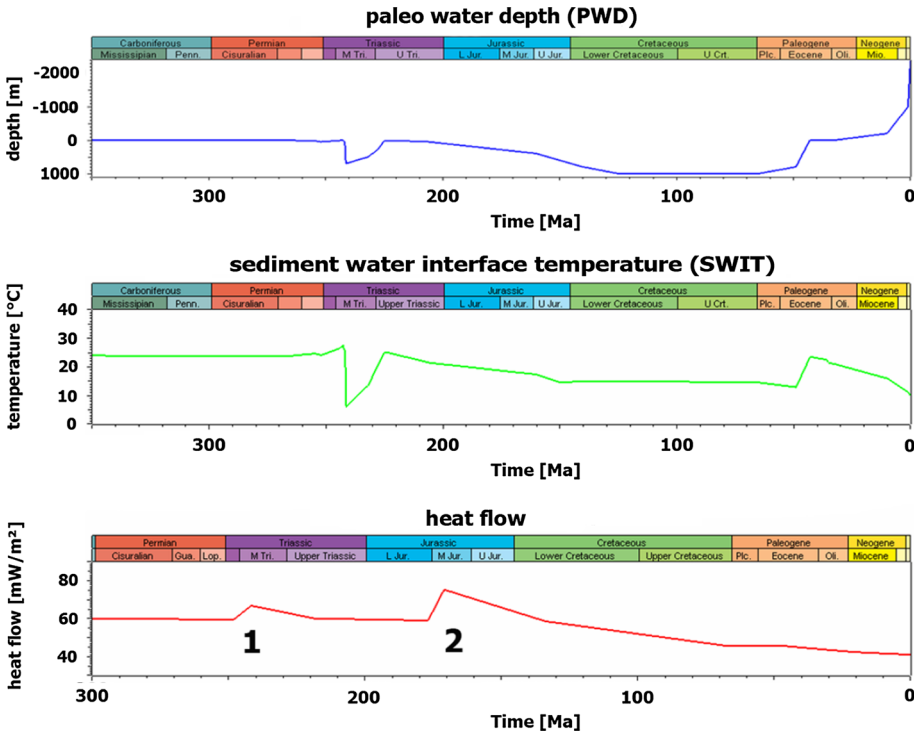

Fig. 5 Paleo water depth (*PWD*), sediment water interface temperature (*SWIT*) and heat flow (*HF*) over time. In the heatflow curve, the rifting of the continental crust (*1*) and the opening of the Ligurian-Piemontese Ocean (*2*) are highlighted

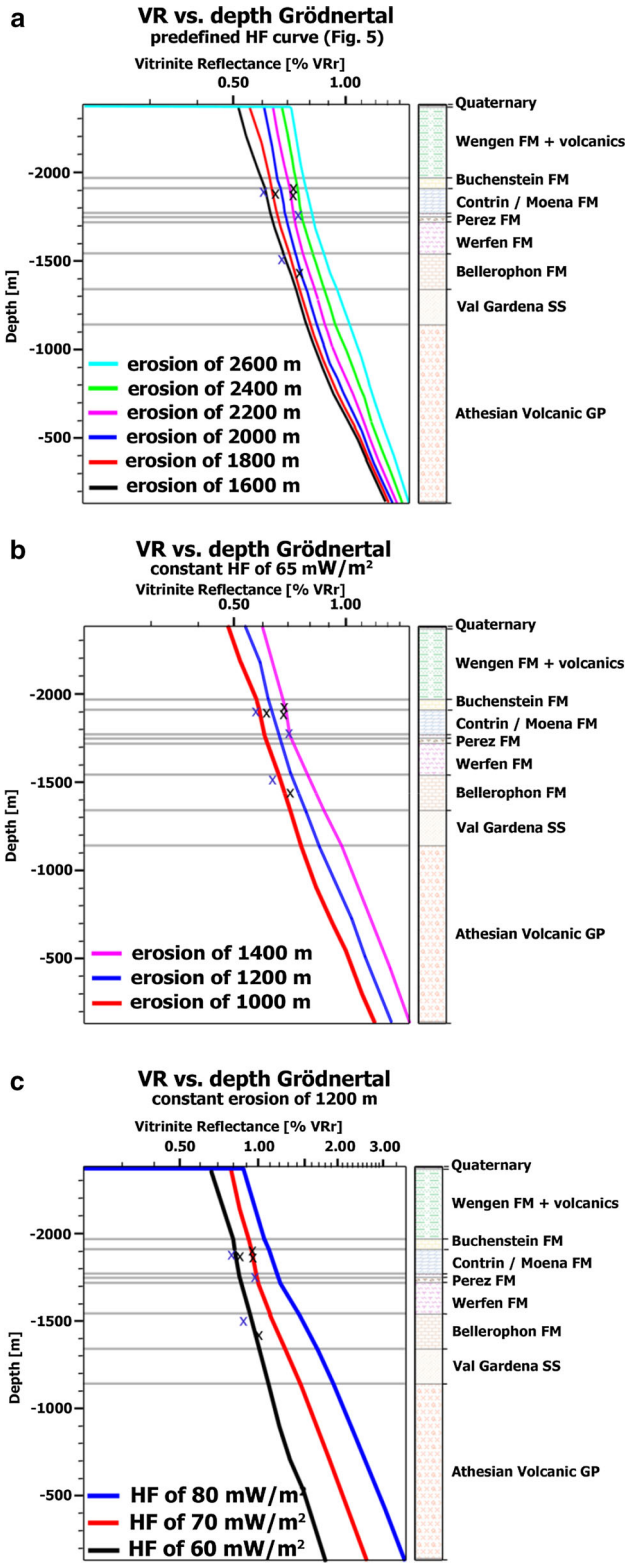

◀**Fig. 6** Results of sensitivity analyses of the Grödnertal model. A second model in the *Frötschbach area* shows same results. Simulated are the predefined HF curve (Fig. 5) with changing eroded thickness (**a**), changing eroded thickness at a fixed HF of 65 mW/m^2, held constantly over time (**b**) and changing constant HFs at a constant eroded thickness of 1200 m (**c**). The *lines* in the plot represent the calculated VR. The VR data used for calibration is indicated by *crosses* (+). Depth is referring to sea level

are shown in Fig. 6. In a first scenario, a best fit case was achieved using the predefined heat flow curve and an optimum thickness for the Cretaceous erosion (Fig. 6a). The plot shows the VR data calculated according to Sweeney and Burnham (1990) as colored lines in comparison with the measured VR data as crosses. With increasing eroded thicknesses the calculated VR lines are shifting to higher VR values, based on a higher paleo overburden and therefore a greater burial depth. As a consequence of the non-constant heat flow curve, the lines are not completely parallel to each other. The best fit curve correlates with an eroded thickness of 1800 ± 200 m. This 'best fit' corresponds to a present day vitrinite reflectance depth gradient of 0.02 % VR_r/100 m, between the top of the Contrin Fm. and the Bellerophon Fm. It should be noted that there is a scatter in the measured vitrinite reflectance values. In such a case, the values showing low reflectance are used for calibration, i.e. the best-fit curve should fit especially the low reflectance values. This procedure takes into account that many samples contain resedimented vitrinites from erosion of older rocks, showing higher reflectances than autochthonous vitrinites.

To illustrate the influence of different eroded thicknesses and different heat flows separately, scenarios b and c are shown in Fig. 6: Scenario b represents a model based on constant heat flow of 65 mW/m^2, which is close to the recent global mean value (Allen and Allen 2005). The lines of the different eroded thicknesses are parallel to each other (Fig. 6b) and shifted to higher VR data with increasing eroded thicknesses. A best fit line is achieved for a thickness of around 1000 m of eroded sediments. The eroded thickness is much lower than in case a, due to higher Cretaceous heat flows. Although a constant heat flow is highly unlikely in view of the complex and variable tectonic setting, scenario b shows that erosional thicknesses have to be treated cautiously.

Scenario c illustrates the use of different heat flows at a constant erosional thickness of 1200 m. Higher VRs are reached with increasing heat flows. Differences are increasing with increasing depth in this case (Fig. 6c).

In addition, an influence of higher heat flow values during the Permian has been analyzed: Even 120 mW/m^2, as maximum value for an assumed rifting (Allen and Allen 2005), during the complete period of the Permian would not increase the present day thermal maturity, as it is overprinted by later burial during the Cretaceous.

Figure 7a shows the burial plot of the *Gardena Valley* model, simulated with the predefined heat flow curve and

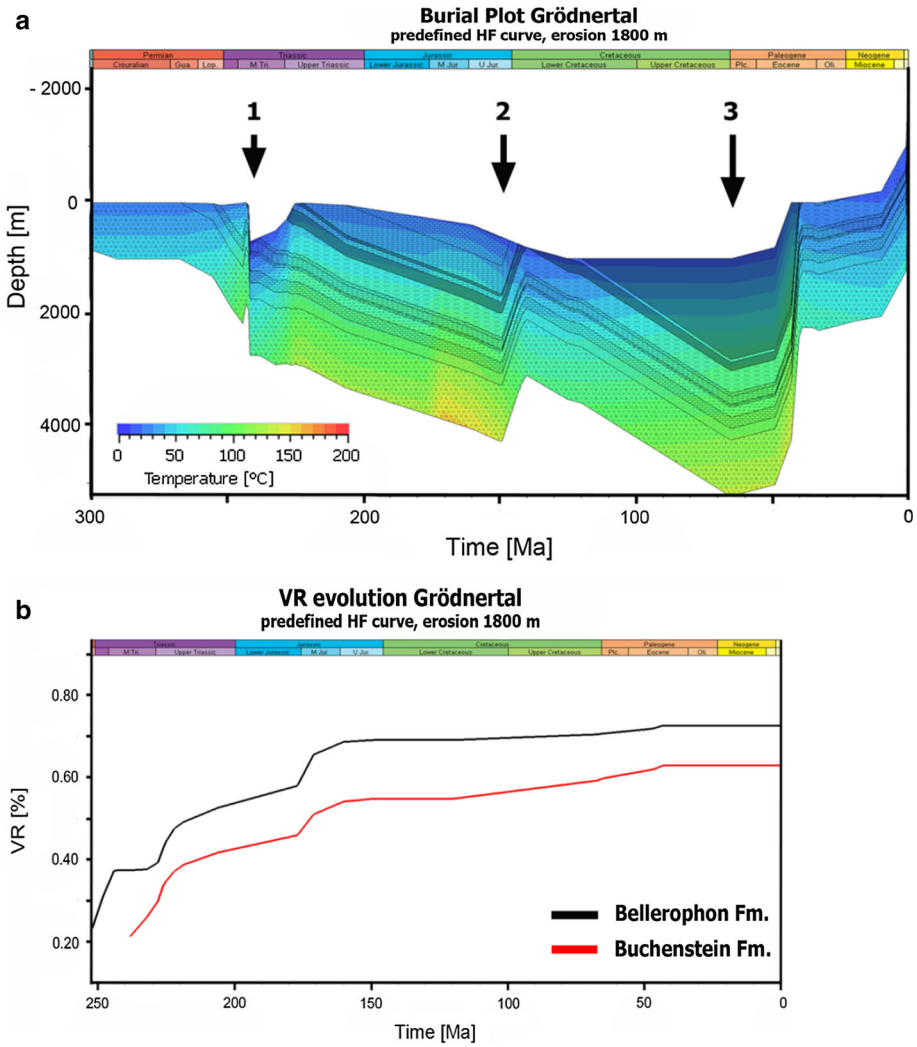

Fig. 7 Burial plot with temperature history of the Gardena Valley model (**a**) and the vitrinite reflectance evolution of Bellerophon and Buchenstein Fm. Simulated with the predefined HF curve and the best fitting eroded thickness of 1800 m (see Fig. 6a)

an eroded thickness of 1800 m for the Cretaceous sediments. The thermal history of the sediments is displayed in this diagram as overlay. Conspicious events shown are the rapid drowning of the basin in the Middle Triassic with a subsequent basin shallowing at constant sedimentation (1) and two phases of major basin inversion (2, 3) aside from the Neogene inversion and uplift. Temperatures reach 158 °C at around 160 Ma before present, with the initiated opening of the Ligurian-Piedmontese ocean, leading to VR values of 1.28 % (2). In addition, the layers were thermally overprinted again 65 Ma before present at the point of deepest burial (160 °C, 1.32 % VR_r) triggered by the sedimentation of the Cretaceous layers.

The vitrinite reflectance vs. time trend (Fig. 7b) shows a clear correlation with the burial trend (Fig. 7a). As temperatures are increasing during times of burial, vitrinte reflectance increases. Due to the fact that the coalification process of vitrinites is irreversable their reflectance is not changing during times of uplift and a second phase of coalification will only be initiated by a second phase of burial provided that previous temperatures are reached or exceeded.

Previous simulations did not include internal radiogenic heat production within sedimentary rocks (e.g. Tscherny 2006). This aspect needs to be kept in mind for a comparison with the new data set of this study. For the Gardena Valley model one simulation was also performed without considering the influence of internal heat production. VR vs. depth trend is shifted to lower VR values, if the internal heat production is neglected. Thus, assumption of more overburden is needed to fit the calculated data with the calibration points of the field data. As a result, the Cretaceous erosion in the Gardena Valley model increases by additional 250–300 m or around 12 % of the total eroded thickness, if the radiogenic heat production is ignored.

4.5 Maturity

The model was calibrated by maturity data measured on samples collected from outcrops. Calibration was performed using VR data ("Appendix"), which were confirmed by T_{max}-values from Rock–Eval analysis. Due to the strong volcanic activities during Ladinian times in the area of the western Dolomites there is some scatter in the data observed (Fig. 6). Nevertheless, the results match largely with published data. As described by Tscherny et al. (2011), VR data for the Middle and Upper Triassic measured in the northern *Gardertal* near Badia by Balzas and Koncz (1999) range between 0.67–1.03 % and VRs measured by Zattin et al. (2003) range between 0.6 and 1.0 %. Tscherny et al. (2011) added own data in the range of 0.6–0.9 % VR. The results of the present study for the *Buchenstein Fm.* (0.61–0.76 % VR_r) agree more with the results of Tscherny (2006) (*Buchenstein*: 0.63–0.75 % VR_r) as compared to those by Zattin et al. (2003), who measured a value of 0.6 % VR_r for the *Moena Fm.* (see Fig. 2).

Reflectance data and sample locations were compared to those of Tscherny (2006). For the samples of the *Buchenstein Fm.* no regional trend of increasing maturity is observed (Fig. 8). Moreover, the comparison shows that the *Buchenstein* data of Tscherny (2006) do not indicate an increase in VR as suggested for other formations from north to south. Slightly increased or decreased VR values could also be explained by changes of sediment thicknesses deposited and by local differences with respect to the influence of tectonic events. For the *Bellerophon Fm.* it seems that a weak increase of VR occurs from west to east. This was suggested by Tscherny (2006) as well, based on his and additional literature data. Furthermore, Emmerich et al. (2008) analyzed sandstones of the *Gröden Fm.* at the *Rosengarten,* around 20 km south of the *Frötschbach* area, and classified VRs higher than 0.9 % VR_r as "not used: proximity to a volcanic dyke". This threshold was confirmed in the present study.

As shown before, maturity levels based on vitrinite reflectance data are basically in good agreement with T_{max} values from Rock–Eval analysis. They vary between 425 and 451 °C. Tscherny (2006) reported T_{max} ranging from 420 to 465 °C. In addition, the samples of Tscherny (2006) represent, like the ones measured here, type II and type III kerogen.

4.6 Burial and temperature history

Summarizing the results from both regional models, an eroded thickness of 1800 ± 200 m of Cretaceous sediments was documented for the northwestern area of the

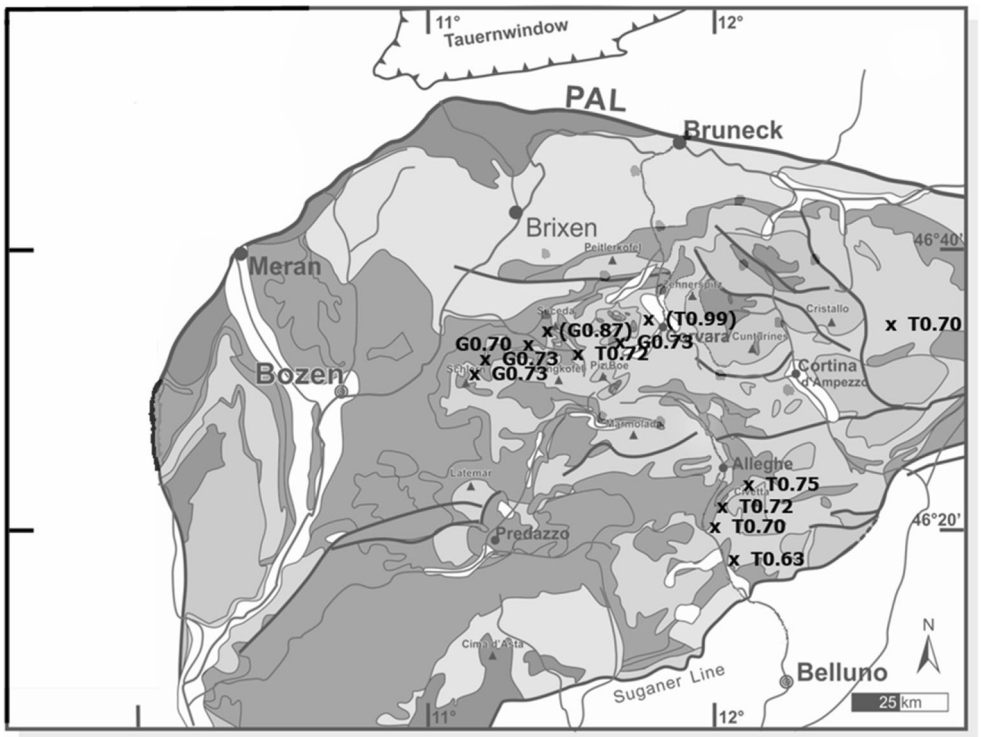

Fig. 8 Regional distribution of VR values of the Buchenstein Formation. *G* is referring to this study and *T* to Tscherny (2006). *Values in parentheses* are regarded as 'too high', possibly influenced by local volcanism or measured resedimented vitrinites

Dolomites combined with a present day maturity gradient of 0.02 % VR_r/100 m. This erosion was initiated by the Alpine Orogenesis starting around 65 Ma and lasting until present day with most rapid uplift at Early Eocene and Late Miocene times. This eroded thickness adds to the eroded thickness of older layers. In the model, it is expected that the eroded Triassic and Jurassic layers were removed during the Late Jurassic (Table 3; Fig. 7a). For our Val Gardena model, we assumed an eroded thickness of pre-Cretaceous units of 500 m, which may be regarded as a maximum scenario. Even if this maximum scenario maturity (vitrinite reflectance) is overprinted by the much larger Tertiary erosional phase. This underlines that even the maximum possible case of Jurassic erosion is not influencing present-day maturity.

Tscherny et al. (2011) published similar results of 1700–2400 m for the Cretaceous erosion with a vitrinite reflectance depth gradient of 0.01–0.02 % VR_r per 100 m. These results were developed on the basis of relatively low heat flows: A peak of 55 mW/m^2 was assigned for the rifting at Jurassic times (160 Ma) and a present day value of 30 mW/m^2. In contrast, this work used 75 mW/m^2 for the Jurassic rifting event and 41 mW/m^2 for the present day value. Based on sensitivity analyses with constant erosion, this slightly higher HF value seems to be more realistic. Heat flows at maximum burial, during the latest Cretaceous, show similar differences with 35 mW/m^2 in Tscherny et al. (2011) and 46 mW/m^2 in this work. It should be noted, that there are varying values published for the Jurassic heat flows as some authors even state very high values of up to 100 mW/m^2 (e.g. Zattin et al. 2003).

Former investigations by Tscherny (2006, without radiogenic heat production and with a present day HF of 41 mW/m^2) result in maximum eroded thicknesses for the Upper Cretaceous of 2000 m (original value of 2300 m prior to correction of internal heat production) and a maturity trend of 0.02–0.03 % VR_r/100 m. Carminati et al. (2010) deduced an erosional thickness of 2200 m for Cretaceous to Paleocene strata, applying relatively high heat flows of 85–105 mW/m^2 during Middle Jurassic times. Thus, their results confirm the estimates of paleo thicknesses presented here. The values of the recent HF are the same in this and in Tscherny (2011, 41 mW/m^2). Ladinian volcanism did not influence maturity of the deepest Triassic and Permian layers or had only local influence (Tscherny 2006).

At this point it should be mentioned that a general increase of maturity could have been influenced by the assumption of overthrusting and later erosion of this tectonical load as well. Doglioni (1985) documented that there are minor overthrusts of Miocene age in the Dolomites. Orogenic loading may have resulted in burial of underlying sedimentary rocks, temperature increase and maturation similar to burial by additional sediments.

5 Conclusions

New vitrinite reflectance data supplemented by solid bitumen reflectance and Rock–Eval data provide important information on thermal maturity of the northwestern Dolomites. Almost all rocks are within the 'oil window', but have not passed the peak oil generation stage (0.9 % VR_r). Exceptions are local areas influenced by volcanism.

The vitrinite reflectance data was used to calibrate temperature and burial history using PetroMod software. Based on these numerical models an eroded thickness of 1800 ± 200 m appears likely for the Cretaceous layers of the study area. The maturity of the *Buchenstein Fm.* ranges from 0.61 to 0.76 % VR_r. This requires a substantial burial and a thicker cover as present today. Times of deepest burial and maximum temperatures presumably correspond to Late Cretaceous/Early Paleocene times. The present day maturity gradient (0.02 % VR_r/100 m) indicates quite a low paleo heat flow situation. After basin inversion was initiated around 65 Ma, the original overburden was eroded during a process of basin uplift. This process mainly took place during the Alpine Orogenesis in Eocene and Miocene times. Burial histories indicate that the influence of deepest burial at around 65 Ma with respect to maturity of Permian and Early Triassic strata overwhelmed earlier temperature events such as high heat flows during the Ladinian.

Nevertheless, it cannot be excluded that the increase of maturity was initiated by overthrusting and later erosion of the overthrusted layer as orogenic loading may have caused the same signal of deepest burial as loading by additional sediments.

Acknowledgments Marco van Veen helped during the sampling campaign in 2013 and Donka Macherey produced high quality polished blocks for vitrinite and solid bitumen reflectance analysis. The text benefited considerably from the great review comments of P. Gianolla and W. Leu.

Appendix

See Table 4.

Table 4 Vitrinite reflectance data

Sample no.	Location	UTM coordinates (32T. *x*/*y*)		Formation	VR_r (%)	St. dev.	Counts	References	T_{peak} (°C)
13/634	Pufels	701471	5160791	Bellerophon	0.70*	–	62	Samples	106.7
13/635	Pufels	701471	5160791	Bellerophon	0.67*	–	66	Samples	103.2
13/639	Pufels	701430	5160576	Perez	0.75*	–	100	Samples	112.3
13/640	Pufels	701385	5160522	Contrin	$1.70^{V.\ std}$	0.435	21	Samples	178.3
13/643	Pufels	701401	5160485	Buchenstein	No VR	–	–	Samples	–
13/648	Pufels	701401	5160485	Moena	0.61	0.103	22	Samples	96.0
13/650	St. Christina	705865	5159593	Buchenstein	0.73*	–	100	Samples	110.1
13/651	St. Christina	705913	5159577	Buchenstein	0.65	0.109	72	Samples	101.2
13/652	St. Christina	705988	5159684	Buchenstein	$1.22^{V.\ std}$	0.348	23	Samples	151.5
13/653	St. Christina	706009	5159601	Buchenstein	0.73	0.095	23	Samples	110.2
13/655	St. Christina	705439	5159962	Bellerophon	0.76	0.086	100	Samples	113.1
13/656	St. Christina	705439	5159962	Bellerophon	0.75	0.097	103	Samples	111.9
13/660	Daunei	710463	5160167	Buchenstein	0.72	0.123	32	Samples	108.8
13/662	Daunei	710328	5160154	Buchenstein	$1.21^{V.\ std}$	0.162	30	Samples	150.9
13/664	Daunei	710347	5160120	Buchenstein	1.03^{V}	0.119	25	Samples	137.9
13/666	Daunei	710800	5160091	Wengen	$1.29^{V.\ std}$	0.190	101	Samples	156.0
13/677	Frommerbach	699311	5157053	Buchenstein	0.76	0.127	100	Samples	113.4
13/678	Frommerbach	699283	5157105	Buchenstein	0.71	0.056	3	Samples	108.3
13/679	Frommerbach	699283	5157105	Buchenstein	0.90	0.059	9	Samples	127.0
13/680	Frommerbach	699259	5157116	Buchenstein	$1.26^{V.\ std}$	0.187	83	Samples	154.1
13/681	Frommerbach	699259	5157116	Buchenstein	$1.75^{V.\ std}$	0.227	18	Samples	180.6
13/683	Frommerbach	699062	5156982	Contrin	0.92	0.067	7	Samples	128.7
13/684	Frommerbach	699010	5157006	Morbiac	0.79	0.147	37	Samples	116.9
13/686	Frötschbach	698515	5155588	Buchenstein	0.61	0.075	100	Samples	96.0
13/687	Frötschbach	698515	5155588	Buchenstein	$0.98^{V.\ std}$	0.151	24	Samples	133.9
13/688	Frötschbach	698515	5155588	Buchenstein	No VR	–	–	Samples	–
13/694	Frötschbach	698691	5155631	Buchenstein	$1.49^{V.\ std}$	0.150	31	Samples	167.6
13/696	Frötschbach	698581	5155639	Buchenstein	0.73	0.140	101	Samples	109.9
13/698	Frötschbach	698581	5155639	Buchenstein	0.50	0.078	66	Samples	79.1
13/699	Frötschbach	698581	5155639	Buchenstein	0.74^{std}	0.178	72	Samples	111.2
13/705	Frötschbach	698581	5155639	Buchenstein	$1.07^{V.\ std}$	0.160	6	Samples	140.9
13/709	Frötschbach	698581	5155639	Werfen	1.29^{V}	0.112	6	Samples	156.0
13/710	Frötschbach	698581	5155639	Werfen	No VR	–	–	Samples	–
13/711	Nova Levante	698581	5155639	Val Gardena	No VR	–	–	Samples	–
13/744	Colfosco	718126	5159610	Bellerophon	0.84	0.038	88	Samples	121.3
13/745	Colfosco	718133	5159607	Bellerophon	0.94^{V}	0.077	96	Samples	130.5
13/755	Colfosco	718393	5159798	Bellerophon	0.94^{V}	0.083	86	Samples	130.5
13/756	Colfosco	718389	5159792	Bellerophon	0.96^{V}	0.066	68	Samples	132.2
13/746	Colfosco	718123	5159614	Morbiac	0.73	0.066	96	Samples	110.0
13/747	Colfosco	718123	5159617	Morbiac	0.77	0.063	39	Samples	114.4
13/749	Colfosco	718196	5159729	Morbiac	0.82	0.083	99	Samples	119.5
13/751	Colfosco	717392	5159620	Buchenstein	0.76	0.086	68	Samples	113.1
05/815	Seceda	707571	5161923	Werfen	0.46	0.086	25	Samples	73.2
05/816	Seceda	708750	5162436	Buchenstein	0.65	0.120	16	Samples	100.6
05/817	Seceda	707464	5161990	Bellerophon	1.01	0.138	20	Samples	136.1
05/820	Seceda	708363	5163103	Buchenstein	0.65^{std}	0.179	25	Samples	100.7
05/930	Geislerspitze/Col Raiser	710077	5160513	Buchenstein	0.66	0.130	22	Samples	101.6

Table 4 continued

Sample no.	Location	UTM coordinates (32T. *x*/*y*)		Formation	VR_r (%)	St. dev.	Counts	References	T_{peak} (°C)
05/931	Geislerspitze/Col Raiser	710502	5159700	Buchenstein	0.72	0.094	20	Samples	109.2
05/932	Geislerspitze/Col Raiser	709029	5161883	Morbiac	0.75	0.107	27	Samples	112.1
Kron3	Würzjoch	715390	5172787	Val Gardena	0.79	0.060	25	Samples	116.5
Kron25	Würzjoch	715593	5171339	Buchenstein	0.63	0.050	46	Samples	98.2
Kron8	Würzjoch	715755	5171512	Morbiac	0.77	0.060	25	Samples	114.4
P6	San Lucano	See reference	See reference	Contrin	0.81	0.070	55	Blendinger et al. (2013)	118.5
P8	San Lucano	See reference	See reference	Contrin	0.82	0.080	50	Blendinger et al. (2013)	119.5
P9	San Lucano	See reference	See reference	Contrin	0.71	0.110	50	Blendinger et al. (2013)	107.9
P600	Pala di San Martino	See reference	See reference	Contrin	0.49	0.044	25	Blendinger et al. (2013)	78.0
P603A	Pala di San Martino	See reference	See reference	Contrin	0.76	0.073	72	Blendinger et al. (2013)	113.4
P603B	Pala di San Martino	See reference	See reference	Contrin	0.73	0.141	67	Blendinger et al. (2013)	110.1
P603C	Pala di San Martino	See reference	See reference	Contrin	0.64	0.123	59	Blendinger et al. (2013)	99.5
P603D	Pala di San Martino	See reference	See reference	Contrin	0.71	0.109	50	Blendinger et al. (2013)	107.9
P324	Pala di San Martino	See reference	See reference	Contrin	0.56	0.158	50	Blendinger et al. (2013)	89.3
P326	Pala di San Martino	See reference	See reference	Contrin	0.56	0.069	39	Blendinger et al. (2013)	89.2
P608	Pala di San Martino	See reference	See reference	Contrin	0.94	0.110	50	Blendinger et al. (2013)	130.5
P85	San Lucano	See reference	See reference	Contrin	$1.55^{V.\ std}$	0.252	12	Blendinger et al. (2013)	170.8
P255	San Lucano	See reference	See reference	Contrin	$1.58^{V.\ std}$	0.163	51	Blendinger et al. (2013)	172.4
P256	San Lucano	See reference	See reference	Contrin	$1.33^{V.\ std}$	0.247	50	Blendinger et al. (2013)	158.5
P316	Pala di San Martino	See reference	See reference	Contrin	0.71^{std}	0.190	52	Blendinger et al. (2013)	107.9
P615	Pala di San Martino	See reference	See reference	Contrin	1.22^{V}	0.115	94	Blendinger et al. (2013)	151.5
P618	San Lucano	See reference	See reference	Contrin	1.58^{V}	0.013	50	Blendinger et al. (2013)	172.4
P606	Pala di San Martino	See reference	See reference	Contrin	$1.15^{V.\ std}$	0.278	50	Blendinger et al. (2013)	146.8
Bb40	Bletterbach	685800	5137100	Val Gardena	0.73	–	–	Buggisch (1978)	110.1
15e	Bletterbach	685800	5137100	Val Gardena	0.60	0.090	–	Bielefeld (1998)	94.3
–	Bletterbach	686750	5136900	Val Gardena	0.88	–	–	Schulz and Fuchs (1991)	125.2
20a	Rosengarten	698900	5142550	Val Gardena	0.76	0.100	–	Bielefeld (1998)	113.4
N6a	Rosengarten	701000	5142350	Val Gardena	0.37	0.140	–	Bielefeld (1998)	55.3
belle	Rosengarten	705014	5145331	Bellerophon	0.52	0.020	–	Emmerich et al. (2008)	82.7

Calculated values based on solid bitumen reflectance measurements after the equation of Schoenherr et al. (2007) are marked with an asterisk (*). Marked values seem to be too high and may be overprinted by volcanism (^{V}) or show a too high standard deviation (^{std})

References

Allen, J. R., & Allen, P. A. (2005). *Basin analysis—Principles and applications* (2nd ed.). Baskerville, Hong Kong, Singapore: Blackwell Publishing Ltd.

Balzas, E., & Koncz, I. (1999). Contribution to thermal evolution of Southern Alps and paleogeographically adjacent areas based on vitrinite reflectance data. *3rd Workshop on Alpine Geological Studies*.

Barker, C. E., & Pawlewicz, M. J. (1994). Calculation of vitrinite reflectance from thermal histories and peak temperatures - A comparison of methods. In P. Mukhopadhyay & W. Dow (Eds.), *Vitrinite reflectance as a maturity parameter* (Vol. 570, pp. 216–229). Washington: American Chemical Society Symposium Series.

Berner, R. A. (1984). Sedimentary pyrite formation: An update. *Geochimica et Cosmochimica Acta, 48*, 605–615.

Bernet, M., Zattin, M., Garver, J. I., Brandon, M. T., & Vance, J. A. (2001). Steady-state exhumation of the European Alps. *Geology, 29*, 35–38.

Berra, F., Jadoul, F., & Anelli, A. (2010). Environmental control on the end of the Dolomia Principale/Hauptdolomit depositional system in the central Alps: Coupling sea-level and climate changes. *Palaeogeography, Palaeoclimatology, Palaeoecology, 290*, 138–150.

Bertotti, G., Picotti, V., Bernoulli, D., & Castellarin, A. (1993). From rifting to drifting: Tectonic evolution of the South-Alpine upper crust from the Triassic to the Early Cretaceous. *Sedimentary Geology, 86*, 53–76.

Bielefeld, D. (1998). Reifebestimmungen an Kohlen des Grödner Sandsteins in Südtirol, unpublished Diploma Thesis. Univ. Cologne.

Bigi, G., Cosentino, D., Parrotto, M., Sartori, R., & Scandone, P. (1990). Structural model of Italy, 1:500.000. CNR—Italian National Research Council.

Blendinger, W. (2004). Sea level changes versus hydrothermal diagenesis: Origin of Triassic carbonate platform cycles in the Dolomites, Italy. *Sedimentary Geology, 169*, 21–28.

Blendinger, W., Bertini, A., Lohmeier, S., & Meissner, E. (2013). Dolomite in the Triassic Dolomites. *Clausthaler Geowissenschaften, 9*, 5–44.

Bosellini, A. (1998). *Geologie Der Dolomiten*. Bozen: Athesia Ges.m.b.H.

Bosellini, A., Gianolla, P., & Stefani, M. (2003). Geology of the Dolomites. *Episodes, 26*, 181–185.

Bostick, N. H., & Foster, J. N. (1975). Comparison of vitrinite reflectance in coal seams and in kerogen of sandstones, shales, and limestones in the same part of a sedimentary section. In B. Alpern (Ed.), *Petrography of Organic Matter in Sediments-Relation to Paleotemperature and Petroleum Potential* (pp. 13–25). Centre National de la Recharche Scientifique, Inter. Collog., Paris, France.

Brandner, R. (1980). Geologische Übersichtskarte von Tirol (1:300.000) & Tektonik (1:600.000). *Tirol Atlas Univ. Verlag Wagner*.

Brandner, R., Keim, L., & Adige, B. (2011). A 4-day geological field trip in the western dolomites. *Geo Alp, 8*, 76–119.

Bruns, B., Di Primio, R., Berner, U., & Littke, R. (2013). Petroleum system evolution in the inverted Lower Saxony Basin, northwest Germany: A 3D basin modeling study. *Geofluids, 13*, 246–271.

Buggisch, W. (1978). Die Grödener Schichten (Perm, Südalpen). Sedimentologische und geochemische Untersuchungen zur Unterscheidung mariner und kontinentaler Sedimente. *Geologische Rundschau, 67*, 149–180.

Carminati, E., Cavazza, D., Scrocca, D., Fantoni, R., Scotti, P., & Doglioni, C. (2010). Thermal and tectonic evolution of the southern Alps (northern Italy) rifting: Coupled organic matter maturity analysis and thermokinematic modeling. *AAPG Bulletin, 94*, 369–397.

Carminati, E., & Doglioni, C. (2012). Alps vs. Apennines: The paradigm of a tectonically asymmetric Earth. *Earth-Science Reviews, 112*, 67–96.

Doglioni, C. (1984). Tettonica triassica transpressiva nelle Dolomiti. *Giornale Di Giologia, 46*, 47–60.

Doglioni, C. (1985). The overthrusts in the Dolomites: Ramp-flat systems. *Eclogae Geologicae Helvetiae, 78*, 335–350.

Doglioni, C. (1987). Tectonics of the Dolomites (Southers Alps, Northern Italy). *Journal of Structural Geology, 9*, 181–193.

Doglioni, C. (1992). Relationships between Mesozoic extensional tectonics, stratigraphy and Alpine inversion in the Southern Alps. *Eclogae Geologicae Helvetiae, 85*, 105–126.

Dunkl, I., Di Giulio, A., & Kuhlemann, J. (2001). Combination of single-grain fission-track chronology and morphological analysis of detrital zircon crystals in provenance studies sources of the Macigno Formation (Apennines, Italy). *Journal of Sedimentary Research, 71*, 516–525.

Emmerich, A., Glasmacher, U., Bauer, F., Bechstädt, T., & Zühlke, R. (2005). Meso-/Cenozoic basin and carbonate platform development in the SW-Dolomites unraveled by basin modelling and apatite FT analysis: Rosengarten and Latemar (Northern Italy). *Sedimentary Geology, 175*, 415–438.

Emmerich, A., Tscherny, R., Bechstädt, T., Büker, C., Glasmacher, U., Littke, R., & Zühlke, R. (2008). Numerical simulation of the syn- to post-depositional history of a prograding carbonate platform: The Rosengarten, Middle Triassic, Dolomites, Italy. *Spec. Publ. International Association of Sedimentology, 40*, 1–36.

Espitalié, J., Deroo, G., & Marquis, F. (1985). La pyrolyse Rock–Eval et ses applications. *Rev. l'Inst. Francais Du Pétrole, 40*, 563–579.

Hantschel, T., & Kauerauf, A. I. (2009). *Fundamentals of basin and petroleum systems modeling*. Berlin, Heidelberg: Springer Verlag.

Hardie, L., & Goldhammer, K. (1986). Repeated subaerial exposure of subtidal carbonate platforms, Triassic, northern Italy: Evidence for high frequency sea level oscillations on a 104 year scale. *Paleoceanography, 1*, 447–457.

Hunt, J. M. (1995). *Petroleum geochemistry and geology* (2nd ed.). New York: W. H. Freeman and Company.

Keim, L. (2008). Geologie im Gebiet Schlern – Seiser Alm : vom Tethysmeer zum Gebirge. *Gredleriana, 8*, 25–46.

Keim, L., Brandner, R., Krystyn, L., & Mette, W. (2001). Termination of carbonate slope progradation: An example from the Carnian of the Dolomites, Northern Italy. *Sedimentary Geology, 143*, 303–323.

Littke, R., Klussmann, U., Krooss, B., & Leythaeuser, D. (1991). Keys to the depositional history of the Posidonia Shale in the Hils syncline, northern Germany. *Geochimica et Cosmochimica Acta, 55*, 3369–3378.

Littke, R., Urai, J. L., Uffmann, A. K., & Risvanis, F. (2012). Reflectance of dispersed vitrinite in Palaeozoic rocks with and without cleavage: Implications for burial and thermal history modeling in the Devonian of Rursee area, northern Rhenish Massif, Germany. *International Journal of Coal Geology, 89*, 41–50.

Lückge, A., Ercegovac, M., Strauss, H., & Littke, R. (1999). Early diagenetic alteration of organic matter by sulfate reduction in Quaternary sediments from the northeastern Arabian Sea. *Marine Geology, 158*, 1–13.

Lückge, A., Horsfield, B., Littke, R., & Scheeder, G. (2002). Organic matter preservation and sulfur uptake in sediments from the continental margin off Pakistan. *Organic Geochemistry, 33*, 477–488.

Lukeneder, A. (2010). Lithostratigraphic definition and stratotype for the Puez Formation: Formalisation of the Lower Cretaceous in the Dolomites (S. Tyrol, Italy). *Austrian Journal of Earth Sciences, 103*, 138–158.

Lukeneder, A., & Aspmair, C. (2006). Stratigrapic Implications of a new Lower Cretaceous ammonoid fauna from the Puez area (Valanginian - Aptian, Dolomites, Southern Alps, Italy). *Geo Alp, 3*, 55–83.

Mählmann, R. F., & Giger, M. (2012). The Arosa zone in Eastern Switzerland: Oceanic, sedimentary burial, accretional and orogenic very low- to low grade patterns in a tectono-metamorphic mélange. *Swiss Journal of Geosciences, 105*, 203–233.

Marocchi, M., Morelli, C., Mair, V., Klötzli, U., & Bargossi, G. M. (2008). Evolution of large silicic magma systems: New U–Pb zircon data on the NW Permian Athesian Volcanic Group (Southern Alps, Italy). *The Journal of Geology, 116*, 480–498.

Masetti, D., Fantoni, R., Romano, R., Sartorio, D., & Trevisani, E. (2012). Tectonostratigraphic evolution of the Jurassic extensional basins of the eastern southern Alps and Adriatic foreland based on an integrated study of surface and subsurface data. *AAPG Bulletin, 96*, 2065–2089.

Massari, F., & Neri, C. (1997). The infill of a supradetachment (?) basin: The continental to shallow-marine Upper Permian succession in the Dolomites and Carnia (Italy). *Sedimentary Geology, 110*, 181–221.

Mundil, R., Brack, P., Meier, M., Rieber, H., & Oberli, F. (1996). High resolution U–Pb dating of Middle Triassic volcaniclastics: Timescale calibration and verification of tuning parameters for carbonate sedimentation. *Planet Science Letters, 141*, 137–151.

Mundil, R., Pálfy, J., Renne, P., & Brack, P. (2010). The Triassic timescale: New constraints and a review of geochronological data. In S. G. Lucas (Ed.), *The Triassic timescale* (pp. 41–60). London: Special Pu. The Geological Society of London.

Nöth, S., Karg, H., & Littke, R. (2001). Reconstruction of Late Paleozoic heat flows and burial histories at the Rhenohercynian-Subvariscan boundary, Germany. *International Journal of Earth Sciences, 90*, 234–256.

Ogg, J. G., Huang, C., & Hinnov, L. (2014). Triassic timescale status: A brief overview. *Albertiana, 41*, 3–30.

Peters, K. E. (1986). Guidelines for evaluating petroleum source rocks using programmed pyrolysis. *AAPG Bulletin, 70*, 318–329.

Peters, K., Walters, C., & Moldowan, M. (2005). *The biomarker guide* (2nd ed., Vol. 1). Cambridge: Cambridge University Press.

Rainer, T., Sachsenhofer, R. F., Rantitsch, G., Herlec, U., & Vrabec, M. (2009). Organic Maturity trends across the variscan discordance in the Alpine-Dinaric transition zone (Slovenia, Austria, Italy): Variscan versus Alpidic thermal overprint. *Austrian Journal of Earth Sciences, 102*, 120–133.

Rantitsch, G., Sachsenhofer, R. F., Hasenhüttl, C., Russegger, B., & Rainer, T. (2005). Thermal evolution of an extensional detachment as constrained by organic metamorphic data and thermal modeling: Graz Paleozoic Nappe Complex (Eastern Alps). *Tectonophysics, 411*, 57–72.

Rullkötter, J., Leythaeuser, D., Horsfield, B., Littke, R., Mann, U., Müller, P. J., et al. (1988). Organic matter maturation under the influence of a deep intrusive heat source: A natural experiment for quantitation of hydrocarbon generation and expulsion from a petroleum source rock (Toarcian shale, northern Germany). *Organic Geochemistry, 13*, 847–856.

Sachse, V. F., Littke, R., Jabour, H., Schümann, T., & Kluth, O. (2012). Late Cretaceous (Late Turonian, Coniacian and Santonian) petroleum source rocks as part of an OAE, Tarfaya Basin, Morocco. *Marine and Petroleum Geology, 29*, 35–49.

Sachsenhofer, R. F. (1992). Coalification and thermal histories of Tertiary basins in relation to late Alpidic evolution of the Eastern Alps. *Geologische Rundschau, 81*, 291–308.

Saeed, M. Al, & Peters, K. (1994). Basin and petroleum system modeling. *Atlantic, 7*, 1253–1262.

Saxby, J. D., Bennett, A. R., Corcorar, J. F., Lambert, D. E., & Riley, K. W. (1986). Petroleum generation: Simulation over six years of hydrocarbon formation from torbanite and brown coal in a subsiding basin. *Organic Geochemistry, 9*, 69–81.

Scheidt, G., & Littke, R. (1989). Comparative organic petrology of interlayered sandstones, siltstones, mudstones and coals in the Upper Carboniferous Ruhr basin, Northwest Germany, and their thermal history and methane generation. *Geologische Rundschau, 78*, 375–390.

Schenk, H. J., Witte, E. G., Littke, R., & Schwochau, K. (1990). Structural modification of vitrinite and alginite concentrates during pyrolytic maturation at different heating rates. A combined infrared, 13C NMR and microscopical study. *Organic Geochemistry, 16*, 943–950.

Schoenherr, J., Littke, R., Urai, J., Kukla, P., & Rawahi, Z. (2007). Polyphase thermal evolution in the Infra-Cambrian Ara Group (South Oman Salt basin) as deduced by maturity of solid reservoir bitumen. *Organic Geochemistry, 38*, 1293–1318.

Schulz, O., & Fuchs, H. W. (1991). Kohle in Tirol: eine historische kohlenpetrologische und lagerstättliche Betrachtung. *Arch. F. Lagerstättenforschung Geol. B.-A., 3*, 123–213.

Senftle, J. T., Landis, R. L., & McLaughlin, R. L. (1993). Organic petrographic approach to kerogen characterization. In M. H. Engel & S. A. Macko (Eds.), *Organic geochemistry* (pp. 355–376). New York: Plenum Press.

Stefani, M., Furin, S., & Gianolla, P. (2010). The changing climate framework and depositional dynamics of Triassic carbonate platforms from the Dolomites. *Palaeogeography, Palaeoclimatology, Palaeoecology, 290*, 43–57.

Stock, H. W. (1994). Stratigraphie, Sedimentologie und Paläugeographie der Oberkreide in den nördlichen Dolomiten (Italien). *Jahrbuch Der Geologischen Bundes-Anstalt, 137*, 383–406.

Suchy, V., Frey, M., & Wolf, M. (1997). Vitrinite reflectance and shear-induced graphitization in orogenic belts: A case study from the Kandersteg area, Helvetic Alps, Switzerland. *International Journal of Coal Geology, 34*, 1–20.

Sweeney, J., & Burnham, A. (1990). Evaluation of a simple model of vitrinite reflectance based on chemical kinetics. *The American Association of Petroleum Geologists Bulletin, 74*, 1559–1570.

Taylor, G. H., Teichmüller, M., Davis, A., Diessel, C. F. K., Littke, R., & Robert, P. (1998). *Organic petrology*. Berlin/Stuttgart: Gebrüder Borntraeger.

Ting, T. C. (1973). Reflectivity of disseminated vitrinites in the Gulf Coast region. Pétrographie de la matière organique des sédiments relations avec la paléotempérature et le potentiel pétrolier. *Centre Nationa de La Recherche Scientifique*.

Tscherny, R. G. (2006). Numerische Simulation der thermischen Evolution und Beckenentwicklung des permo-mesozoischen Südalpins (Dolomiten) entlang der TransAlp-Traverse. *Dissertation RWTH Aachen University (ISBN 3-86130-828-2; German with English Abstract)*.

Tscherny, R. G., Büker, C., Nöth, S., Uffmann, A. K., & Littke, R. (2011). Coalification of dispersed organic matter in the Dolomites, Italy: Implications for burial and thermal history. *Geo Alp, 8*, 4–19.

Winterer, E., & Bosellini, A. (1981). Subsidence and Sedimentation on Jurassic Passive Continental Margin, Southern Alps, Italy. *AAPG Bulletin, 65*, 394–421.

Zattin, M., Cuman, A., Fantoni, R., Martin, S., Scotti, P., & Stefani, C. (2003). Thermochronological evolution of the eastern Southern Alps from vitrinite reflectance and fission track data. *Atti Ticiensi Di Scienze Della Terra, 9*, 92–95.

Zattin, M., Stefani, C., & Martin, S. (1990). *Detrital fission-track analysis and sedimentary petrofacies as keys of Alpine exhumation: The example of the Venetian foreland*. Italy: European Southern Alps.